Mechanical Imaging of a Volcano Plumbing System From GNSS Unsupervised Modeling

François Beauducel, Aline Peltier, Antoine Villié, Wiwit Suryanto

AGU ADVANCING EARTH AND SPACE SCIENCE

Geophysical Research Letters

RESEARCH LETTER
10.1029/2020GL089419

Mechanical Imaging of a Volcano Plumbing System From GNSS Unsupervised Modeling

François Beauducel[1,2], Aline Peltier[1,3], Antoine Villié[4], and Wiwit Suryanto[5]

[1]Institut de physique du globe de Paris, Université de Paris, CNRS, Paris, France, [2]Université Grenoble Alpes, Université Savoie Mont Blanc, CNRS, IRD, IFSTTAR, ISTerre, Grenoble, France, [3]Observatoire Volcanologique du Piton de la Fournaise, IPGP, La Réunion, France, [4]Laboratoire de biométrie et biologie évolutive, CNRS UMR, Villeurbanne, France, [5]Geophysics Research Group, Universitas Gadjah Mada, Yogyakarta, Indonesia

Abstract Identification of internal structures in an active volcano is mandatory to quantify the physical processes preceding eruptions. We propose a fully unsupervised Bayesian inversion method that uses the point compound dislocation model as a complex source of deformation, to dynamically identify the substructures activated during magma migration. We applied this method at Piton de la Fournaise. Using 7-day moving trends of Global Navigation Satellite System (GNSS) data preceding the June 2014 eruption, we compute a total of 15 inversion models of 2.5 million forward problems each, without a priori information. Obtained source shapes (dikes, prolate ellipsoids, or pipes) show magma migration from 7–8 km depth to the surface, drawing a mechanical "tomography" of the magma pathway. Our results also suggest source geometries compatible with observed eruptive fissures and seismicity distribution. In case of finite magma volume involved in final dike injection, source volume estimates from this method allow forecasting volumes of erupted lava.

Plain Language Summary Imaging the interior of an active volcano and estimating volumes of magma present at depth are major challenges of eruption anticipation. In this work we propose an effective method of data processing that combines a mathematical model of the potential source at depth and standard ground deformation measurements at the surface in a fully automated process that has been implemented as a real-time monitoring tool to anticipate eruptions at Piton de la Fournaise volcano. The method is sensitive to magma migration, highlighting the magma pathway, like a scanner that displays a 3-D image of the volcano plumbing system. In specific circumstances, this method can be used also to forecast volumes of erupted lava.

Key Points:
- Unsupervised GNSS modeling offers fast detection and volume estimate of migrating magma
- Deformation source modeling draws a mechanical tomography of the volcano internal substructures
- Full model space Bayesian inversion serves as a robust real-time monitoring tool

Supporting Information:
- Supporting Information S1
- Movie SI

Correspondence to:
F. Beauducel,
beauducel@ipgp.fr

Citation:
Beauducel, F., Peltier, A., Villie, A., & Suryanto, W. (2020). Mechanical imaging of a volcano plumbing system from GNSS unsupervised modeling. *Geophysical Research Letters*, *47*, e2020GL089419. https://doi.org/10.1029/2020GL089419

Received 19 JUN 2020
Accepted 16 AUG 2020
Accepted article online 21 AUG 2020

1. Introduction

Active volcano edifices can deform due to fluid migration and storage into their so-called plumbing system, an interconnected network of internal volumetric substructures like reservoirs, conduits, or sills/dikes (Tibaldi, 2015). Indeed, fluid dynamics into the plumbing system involves mechanical constraints (pressure, volume, or stress variations) that are applied to the internal boundaries of the medium, inducing deformation that usually reach the free ground surface. As a result, monitoring volcano deformation is commonly used to detect the subtle warning signals of a volcanic eruption linked to the pressurization of magma body or magma transfers at depth (see Dzurisin, 2003 for a review and Segall, 2010 for method limitations). Furthermore, inversion of the geodetic data with mechanical models has natural capability to locate the pressure source in depth and to quantify its characteristics from surface observations, notably its volume variation that can be an estimate of magma volume in depth (see, for instance, Anderson et al., 2010; Beauducel et al., 2004; Cayol & Cornet, 1998; Peltier et al., 2016; Toutain et al., 1992). Any quantitative volcano model needs boundary conditions, in particular those common to the magma fluid dynamics and the volcano mechanical behavior, that is, the plumbing system geometry. Imaging these structures using various tomography methods has the main goal of describing, in a more quantitative way than geological approaches, the internal structures, which might be used in other geophysical or geochemical dynamic modeling as a priori information. In this context, the characterization of the magma feeding system (location, volume, shape, etc.) with short-term and reliable quantitative parameters is also an important prerequisite for understanding and anticipating any eruptive activity.

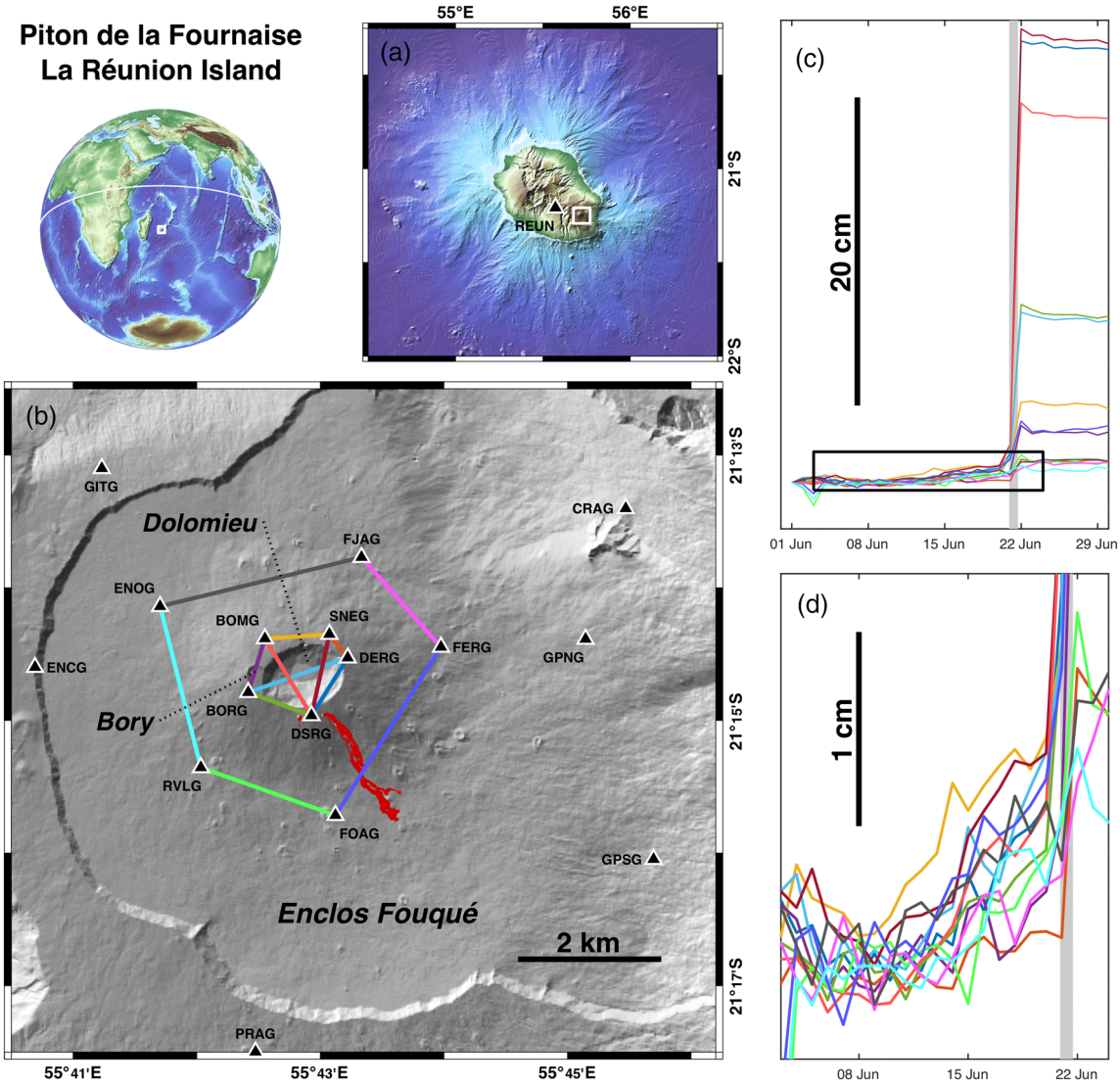

Figure 1. (a) Location map of La Réunion Island and reference station; (b) Zoom on the most active part of Piton de la Fournaise and summit craters. GNSS permanent stations (black triangles), June 2014 lava flows (solid red patch), and selected baselines (color solid lines) are shown; (c) baseline variations (i.e., distance changes between pairs of stations) on the preeruptive, coeruptive, and posteruptive periods (same colors as in b); (d) zoom on the preeruptive precursory baseline variations. Gray area indicates eruption time. Topographic data from ETOPO1, SRTM, SHOM, and RGEALTI IGN 2016.

In this work, we follow the magma circulation and/or accumulation in depth by locating and quantifying pressurization sources in space and time using unsupervised deformation source modeling from Global Navigation Satellite System (GNSS) observations at Piton de la Fournaise (PdF, La Réunion Island, Indian Ocean, Figure 1a). We introduce here the innovative term of mechanical tomography, since the method uses magma ascent as an active source that progressively illuminates the complex magma plumbing system and finally gives an image of the internal substructure geometries that have been activated during the PdF unrest.

PdF is a 2,632 m high active basaltic volcano, often in eruption with an average of two eruptions per year since the creation of the Observatoire Volcanologique du Piton de la Fournaise (OVPF/IPGP) in 1979. Recent eruptions mainly occured inside an uninhabited caldera, called Enclos Fouqué, where a terminal cone topped by two craters (Bory and Dolomieu), gradually built up (Figure 1b).

The location and the shape of the shallow magma reservoirs below the volcano are still debated even if recent geodetic, seismic, and geochemical studies converge toward a conceptual model of a plumbing system constituted of several reservoirs, variably connected and distributed from 10 km depth to the near-surface (Battaglia et al., 2005; Boudoire et al., 2019; Di Muro et al., 2014; Peltier et al., 2009). Passive *S* and *P* wave

tomographies made on PdF, using ambient seismic noise and *P* wave first arrival times for earthquakes, respectively, show (1) a high *S* wave velocity zone from 0.7 to 1.6 km above sea level, a.s.l. below the terminal cone interpreted as a preferential path for magma injections (Brenguier et al., 2007) and (2) a high-velocity plug at sea level, under the summit craters, interpreted as an intrusive, solidified dike-and-sill complex with little fluid magma storage (Prôno et al., 2009). Two low *P* wave velocity anomalies, which may highlight magma reservoirs, are found from 0 to 1 km a.s.l. and from 1 to 2 km b.s.l. (Prôno et al., 2009). At greater depth, spatiotemporal distribution of the seismicity may evidence the presence of a deeper reservoir at around 7.5 km depth below sea level (b.s.l.) (Battaglia et al., 2005; Peltier et al., 2009).

The long-term preeruptive edifice inflation is often of very low amplitude at PdF (often less than 5 cm in one month; e.g., in Peltier et al., 2016, 2018). On 9 June 2014 (all dates and times UTC), after an unusually long period of 41 months of dormancy and slow deflation, PdF showed signs of unrest with the start of a slow edifice inflation and an increase of the shallow (<2 km depth) seismic activity. Two seismic crises (not associated with detectable ground deformation) occurred on 13 and 17 June, with 360 and 687 shallow volcano-tectonic earthquakes, respectively. A third seismic crisis that lasted 1 hr and 16 min (888 shallow volcano-tectonic earthquakes located between 0.3 and 1.5 km a.s.l., below the Dolomieu crater and associated with significant ground deformationof 20 cm maximum) led to an eruption on 20 June, 21:35. The eruptive fissures opened on the external and south southeastern slope of the Dolomieu crater (2,348–2,480 m elevation; Figure 1b). Eruptive activity ended on 21 June, 17:09 and emitted about $0.4 \pm 0.2 \times 10^6$ m^3 (no DRE) of lava flows (Peltier et al., 2016).

2. Methods

2.1. GNSS Data Processing

Among other multidisciplinary networks, OVPF maintains 24 permanent GNSS stations, one of the most dense networks at an active volcano. Raw data are processed using PPP method by the Gipsy-Oasis software (Desai et al., 2014) providing daily solutions in the ITRF2008 reference frame. The typical standard deviations over 5 year period has been estimated at a station located 15 km from the summit and not affected by volcano deformation (REUN, Figure 1a), and equal to 5.2, 4.8, and 11.2 mm for eastern, northern, and vertical components, respectively. We removed horizontal tectonic motion from the time series using linear velocity trend estimated from this station, with values of +18 mm/yr eastern and +12 mm/yr northern.

In order to increase the signal-to-noise ratio of GNSS observations, we compute displacement trends over a 7 day moving-window. Estimating ground velocities over a few days' sliding sample window increases the sensitivity to detect subtle signals below the error level of individual daily solutions while preserving the temporal resolution required to capture magmatic processes. Typically, the error on a 7-day velocity trend is as low as about 0.14 mm/day, that is, only 0.8 mm on the displacement.

For this study, due to random noisy signal at some distal stations, we used the 10 stations located within a 4 km radius from the summit, where baseline variations were mostly significant during the June 2014 unrest (Figure 1). We checked that the far-field displacements remain correctly constrained by the five stations located at the bottom of the terminal cone (see Text S2 in the supporting information).

2.2. pCDM Method

The point compound dislocation model (pCDM), proposed by Nikkhoo et al. (2016), provides analytical expressions for surface displacements due to a source composed of three mutually orthogonal tensile point dislocations: one horizontal and two vertical, freely oriented in space (i.e., three rotational degrees of freedom around each 3-D axis) in an elastic homogeneous half-space. Original equations depend on nine source parameters: three for the hypocenter location (horizontal coordinates and depth), three volume variations dV_X, dV_Y, and dV_Z (of the same sign, for each plane perpendicular to its axis), and three for the angles of rotations ΩX, ΩY, ΩZ (see Figure 2). A tenth parameter is the Poisson's ratio that we fixed to 0.25 to consider an isotropic medium. Since equations use the volume dislocation for the deformation source and not the pressure, the model is independent from other elastic parameters.

In order to express the total volume dislocation ΔV, an easier quantitative parameter for interpretation, we substituted the three volume variations variables with their total value plus two dimensionless shape ratios between 0 and 1, defined as follows:

$$\Delta V = dV_X + dV_Y + dV_Z, \quad (1)$$

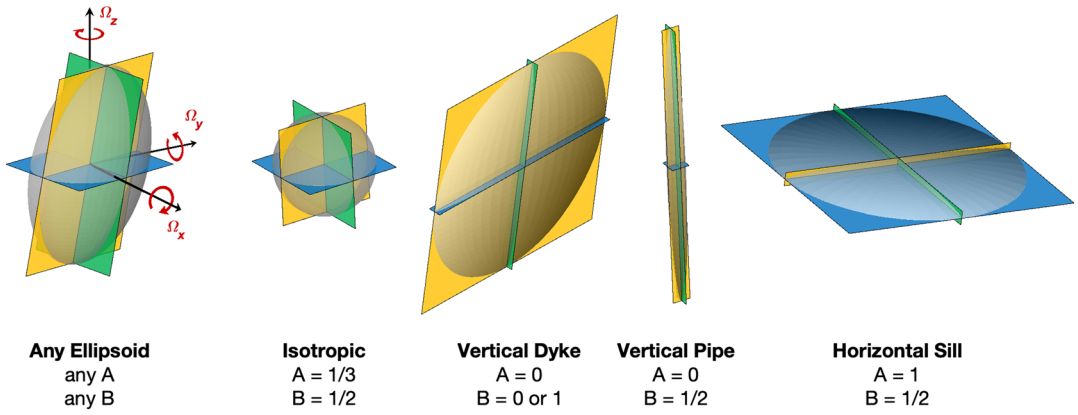

Figure 2. pCDM dislocation plans and rotation angles definition. Example of source shapes and the associated A and B values. Surface of each point dislocation is enlarged to be proportional to its associated volume variation.

$$A = \frac{dV_Z}{\Delta V}, \tag{2}$$

$$B = \frac{dV_Y}{dV_X + dV_Y}, \tag{3}$$

where ΔV is the total volume variation of the source, A is the horizontal over total volume variation ratio, and B is the vertical volume variation ratio.

The pCDM is able to approximate any shape of magma bodies, as dikes, sills, oblate, prolate, and other triaxial ellipsoidal shapes (see some examples with corresponding A and B values in Figure 2), and is only relevant at far-field observation points because of the point source approximation. Even if simple, this model is particularly well adapted for real-time monitoring as it gives a first-order estimation of the volume and shape of the source(s) at the origin of the surface displacements, yet is still easy to implement in an inverse problem.

We also rewrote the original pCDM code in a fully vectorized way (Matlab/GNU Octave and C languages) in order to make it compatible with fast inversion with millions of forward problems, and allow formulations to approximate topographic effects (varying-depth method proposed by Williams and Wadge (1998), that is, adjusting the source depth at each observation point using station elevation), and express the source depths relative to sea level.

2.3. Inverse Problem

In order to obtain a description as objective as possible of the volcano internal structures responsible for the surface displacements, we minimize the a priori information and explore the entire space of the nine model parameters using the GNSS trends as observation data. As a first result of this unsupervised inversion method, we represent the model space probability as a function of source location, to display all solutions that are consistent with observations (Tarantola, 2006). Identification of a single volume zone with higher probabilities confirms the existence of a cluster of good models, a mandatory condition to possibly select one best model.

Since exhaustive grid exploration of the full model space is not reasonable with nine parameters, we use a Monte Carlo Bayesian parallel algorithm with five iterations, each using 500,000 forward problems randomly chosen in the model space with possible reduction of search interval between iterations. Each iteration performs uniform sampling except for horizontal position for which we use a normally distributed sampling centered at the summit with a 5-km standard deviation radius. This a priori information improves the inversion performance as we are expecting source in the neighborhood of the summit area but does not exclude any possible distant nor deep source location. Misfits are calculated using the L1 norm between observed and modeled data. For each iteration, if the marginal distribution has a single significant maximum probability mode, the process selects a smaller range for this parameter with higher probability to constrain the

best models for the next iteration. A posteriori uncertainties of the best model solution are then given by the interval of variation over each parameter that keeps 68% (1 standard deviation) of the highest model probabilities for all the iterations, a total of 2.5 million forward models.

Since the method uses a single source as forward problem, only the dominant source, that is, the one that induces the maximum amplitude displacements at surface, will be identified by the inverse problem. As a consequence, the main source of deformation might hide other simultaneous active sources of lower amplitude, eventually with opposite sign of volume variation.

3. Results

First signs of inflation at PdF appeared on 9 June 2014 (Figures 1c and 1d), and accelerated after 13 June, with a summit extension well visible on the DSRG-SNEG baseline (see dark red line in Figure 1d). The amplitude of the ground deformation preceding the 20 June 2014 eruption remained particularly low, that is, less than 1 cm of horizontal cumulative displacements and about 2 cm maximum of vertical cumulative displacements recorded on the summit stations in 11 days. These low intensity of surface observations makes this eruption a good case study for developing high-sensitivity modeling methods.

Results of the inversion modeling for 15 periods (12 before and 3 after the eruption) of 7 day sliding sample window provide the position and the shape of the pressure source through time. Figure 3 shows results of each inversion like a full description of the model space probabilities as marginal distributions in horizontal and vertical projections (see also Table S1 in the supporting information). Three distinct preintrusion phases (Phases 1–3) before the final dike propagation to the surface (Phase 4) can be distinguished.

(1) For the windows spanning 2–8, 3–9, 4–10 and 5–11 June, no well-constrained source can be found but probable deep deflation diffuse sources seem to be present below the terminal cone.
(2) Inflation sources appeared and became more consistent from the 6–12 June period with a narrower range of models and a best inflation source located at 4.5 km b.s.l., i.e. about 7 km below the summit, with a tilted dike shape. The inflation pressure source, the shape of which evolves from a dike to a pipe, remained deep (0 to 3 km b.s.l.) until 16 June.
(3) From the 11–17 June to the 13–19 June periods, when the deformation rate accelerated, the inflation source was shallower, located between 0.7 and 1 km a.s.l. (i.e., between 1.8 and 1.5 km below the summit). The last pressure source modeled before the eruption, for the period spanning 13 to 19 June, displayed a volume variation of +210,000 m^3.
(4) On 20 June, the 1 hr and 16 min seismic crisis associated with rapid ground deformation(Figure 1c) marked the final magma dike propagation to the surface that fed the eruption. The shape of the dike appeared in our models only from the 16–22 June sliding window. For the two previous periods (14–20 June and 15–21 June), the best models were ellipsoid sources, probably because of the influence of two sources (the preeruptive source and the final dike) associated with the integrating effect of the 7-day trend calculation. Volume variations for the two last coeruptive periods (15–21) and (16–22) were relatively constant, with values of +230,000 m^3 and +300,000 m^3, respectively.

4. Discussion

Even with <1 cm ground displacements, we are able to image the refilling of the shallow magma plumbing system preceding the June 2014 eruption at PdF. Our previous attempts to identify preeruptive magma migration using deformation data may have failed because of the use of too simple isotropic sources as primary models. The success of the inversion using more complex model suggests deformation sources at PdF often with flat or elongated shapes, like dikes or pipes.

First signs of deep fluid upward (from mantle level) preceding the June 2014 eruption have been evidenced in March-April 2014 by mantellic eccentric seismicity and soil CO_2 anomalies on the western outer volcano flank, more than 10 km from the summit (Boudoire, Liuzzo, et al., 2017, Boudoire, Di Muro, et al., 2017). During that time and until early June 2014, seismicity below the terminal cone remained low and only a slight edifice deflation was observed. The first models (Phase 1, 2–11 June) show deep deflation sources before the magma migration starts (Figures 3 and 4). This volume loss might correspond to the emptying of deeper reservoir(s) before the magma starts to "drill" and follows a path to shallower levels (Phase 2; Figure

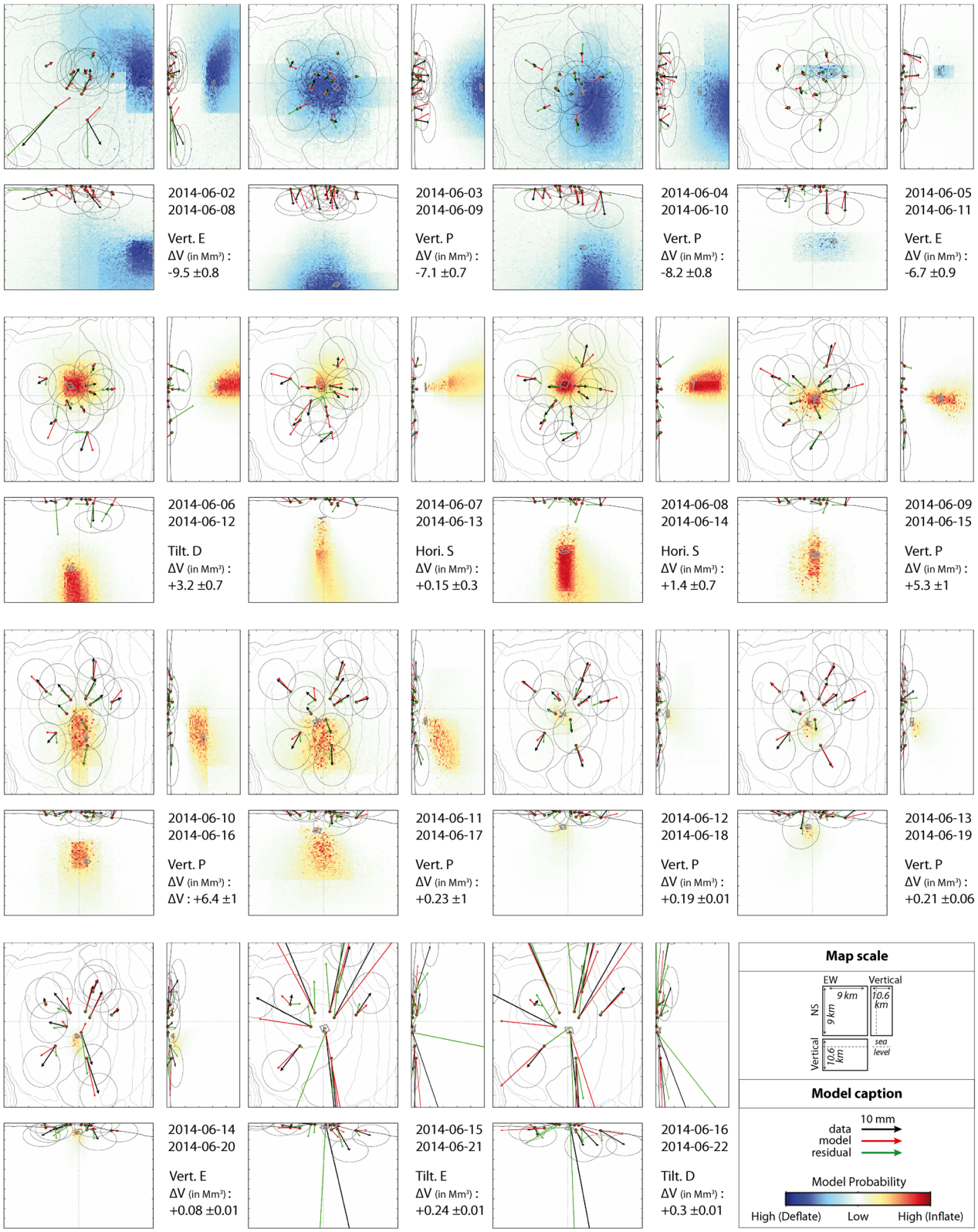

Figure 3. Temporal evolution of the daily pCDM source solution from Bayesian inversion of 7-day displacement trends from 8 to 22 June 2014, in map and vertical cross-section views. Time interval of each model is given in the figure. Color map indicates the maximum probability level combined with the volume variation sign (yellow-orange-red for inflation, green-cyan-blue for deflation). Black, red, and green arrows are observed displacements, modeled displacements and residual, respectively. Ellipses are errors. Best model source location and shape are indicated as gray plans, and their source approximate shape (E: Ellipsoid, S: Sill, P: Pipe, D: Dike) and volume variation (M m^3) are indicated.

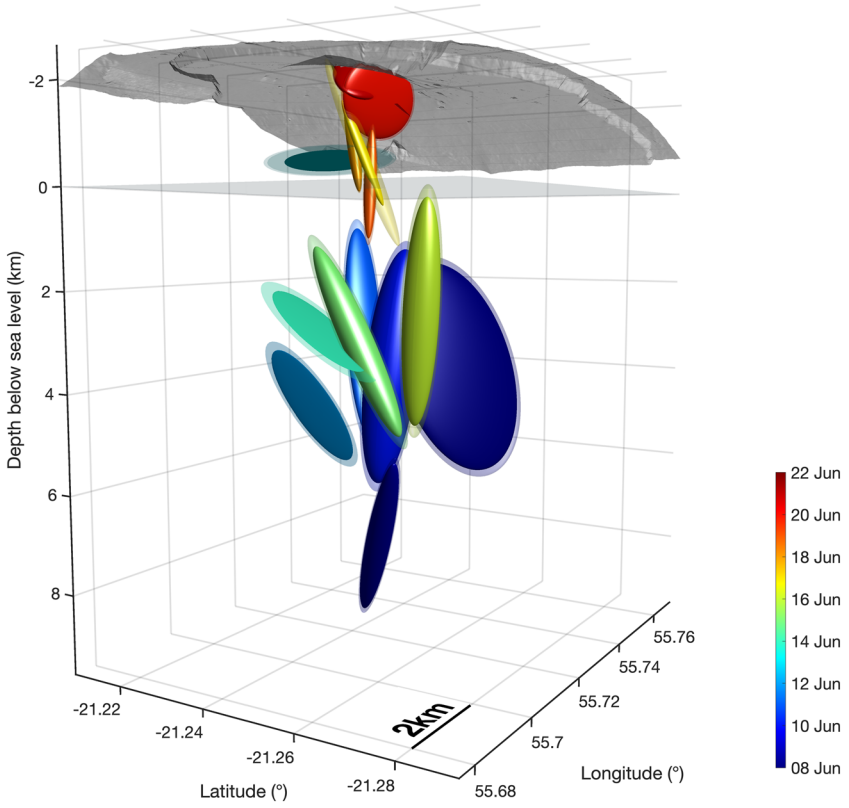

Figure 4. Synthetic and virtual 3-D view of the different best models identified during the June 2014 preeruptive unrest at Piton de la Fournaise. Colors stand for the most recent date of each time window. Size of each source is proportional to its associated volume variation. Transparent plan at depth = 0 simulates the sea level.

4). On Phase 2, our results suggest increasingly shallow sources of overpressure from 12 June 2014 (Figure 4). It started from 7 to 8 km b.s.l. (at the lower limit of our model space) where a reservoir has already been inferred from seismicity in 1998 (Battaglia et al., 2005), up to 1.5 km a.s.l., where the shallower reservoir is suspected to lie (1.3 to 1.9 km depth below the summit Peltier et al., 2016). Most of the pressure sources below sea level are vertically elongated and seems to highlight the volcano deep conduit connecting the two reservoirs, forming a continuum more or less filled by fluids (Figures 3 and 4). Rather than tracking the details of magma migration, which would require a higher time sampling frequency, we imaged the PdF plumbing system (from about 10 km depth to the surface; Figure 4). The synthetic 3-D view of the different sources identified during the June 2014 preeruptive unrest shows a gap at sea level, at the same level where Prôno et al. (2009) describe a high-velocity plug interpreted as a solidified complex with little fluid storage, and where Battaglia et al. (2005) describe a discontinuity in the upward migration of the seismicity preceding the 1998 eruption. Following the 1998 eruption, most of the deep recharges were not accompanied by deep seismicity, the majority of the earthquakes being located above sea level (Duputel et al., 2019; Lengliné et al., 2016). This suggests a generally deep open conduit, which fed the 34 eruptions between 1998 and 2014 (Roult et al., 2012). Our results illustrate the value of geodetic monitoring when the shallow system is already open, and seismic activity absent. The first models (Phase 1) show deep deflation sources before the magma migration starts (Figures 3, 4). This volume loss might correspond to the emptying of a deeper reservoir(s) before the magma starts to "drill" and follows a path to shallower levels (Phase 2; Figure 4). For Gurioli et al. (2018), the products emitted during the eruption came from a shallow, differentiated magma source, already in place since 2009 that has been re-activated by fast volatile ex-solution and crystal-melt separation. The migrating sources we modeled display significant volume variation that probably involve more than only gas and highlight new magma upward migration up to 1.5 km depth. Source locations during Phase 3 suggests that the fracturing that the final dike (Phase 4) started from about 1.5 km depth below the southern border of the Dolomieu crater (Figures 3 and 4). The two seismic crises, on 13 and 17 June, with earthquakes above sea level, show already shallow pressure source(s) at that time.

Our estimated source volume variations are relatively constant during Phases 3 and 4, that is, around 0.25 M m^3 (Figure 3) despite the displacement increasing over 1 order of magnitude between preeruptive and syneruptive periods. This volume consistency indicates only a limited volume of magma involved in the final phase of magma migration. However, if we had used an isotropic source, this process could not have been properly modeled as for a given depth, the volume variation must be proportional to surface displacements. Using pCDM, the source shape has the capability to be adjusted while keeping a constant volume variation and maintaining a shallow depth. In addition, the final volume variation is of the same order of magnitude as the one obtained using an isotropic source for the whole coeruptive period (130,000 to 190,000 m^3 Peltier et al., 2016), and close to the real erupted volume of 0.4 ± 0.2 M m^3, that is, a DRE volume of 0.17–0.28 assuming a porosity range of 30–58% (Di Muro et al., 2014).

In spite of the elastic and homogeneous assumptions for the models, the volume variation obtained from deformation and erupted volume are consistent for short-lived eruptions not sustained by additional dike refilling. We demonstrate with our modeling the need of looking at shorter time periods to evidence migration processes and complex internal shallow structures. GNSS daily solutions are certainly a limitation in this context, and higher frequency may help in identification of finer structures.

5. Conclusion

The low-amplitude surface displacements preceding the 20 June 2014 eruption at PdF makes this eruption a good case study for developing and validating high-sensitivity modeling methods. Our work provides new insights into the refilling of the shallow magma reservoir the days preceding the eruption. The pCDM method we used allows the tracking of magma from depth to the upper reservoir, and the final dike propagation to the surface, by discriminating both the shape, location and volume of the successive modeled sources. The rewriting of the original pCDM code in a fully vectorized way allows for fast inversion and easy implementation to provide rapid first-order modeling results and assist crisis management. Similar to the results obtained at Mount Etna by Cannavò et al. (2015), our method is fast and fully unsupervised, without a priori information on the source parameters except the choice of the pCDM itself. In view of these promising results, we implemented this method operationally as an extension of the GNSS module in the WebObs system (Beauducel et al., 2020), an integrated web-based system for data monitoring and network management implemented in 15 observatories worldwide. The module was initially developed with a simple isotropic point source (Beauducel et al., 2014, 2019), and we added the possibility of setting a pCDM source and associated parameters for real-time modeling. This has been especially useful during recent crisis managements at La Soufrière de Guadeloupe (Moretti et al., 2020) and PdF.

Data Availability Statement

GNSS raw data are available at https://volobsis.ipgp.fr, processed data by contacting OVPF-IPGP. WebObs system is an open-source project available at this site (https://github.com/IPGP/webobs).

Acknowledgments
This work is a tribute to F. B.'s late thesis supervisor François H. Cornet. Authors warmly thank Mehdi Nikkhoo for sharing his revolutionary analytical model. Many thanks to the University of Gajah Mada, the IRD in Jakarta, and the Indonesian Ministry RistekDikti for having supported the project. We thank the OVPF staff for high quality data collection. This work has been supported by a Grant from Labex OSUG@2020 (Investissements d'avenir ANR10 LABX56) and EUROVOLC project that received funding from the European Union's Horizon 2020 research and innovation programme under Grant Agreement 731070. This is IPGP contribution 4159. Many thanks to an anonymous reviewer and to Nico Fournier for useful comments and suggestions.

References

Anderson, K., Lisowski, M., & Segall, P. (2010). Cyclic ground tilt associated with the 2004–2008 eruption of Mount St. Helens. *Journal of Geophysical Research*, *115*, B11201. https://doi.org/10.1029/2009JB007102

Battaglia, J., Ferrazzini, V., Staudacher, T., Aki, K., & Cheminée, J.-L. (2005). Pre-eruptive migration of earthquakes at the Piton de la Fournaise volcano (Réunion Island). *Geophysical Journal International*, *161*(2), 549–558.

Beauducel, F., De Natale, G., Obrizzo, F., & Pingue, F. (2004). 3-D modelling of Campi Flegrei ground deformations: An example of trade-off between source and structure. *Pure and Applied Geophysics*, *161*(7), 1329–1344.

Beauducel, F., Lafon, D., Béguin, X., Saurel, J.-M., Bosson, A., Mallarino, D., et al. (2020). WebObs: The volcano observatories missing link between research and real-time monitoring. *Frontiers in Earth Science*, *8*, 48. https://doi.org/10.3389/feart.2020.00048

Beauducel, F., Nandaka, M. A., Syahbana, D. K., Suryanto, W., Nurnaning, A., Iguchi, M., et al. (2019). Real-time magma flux quantization from GNSS as a tool for crisis management. In *VOBP4, Mexico City, November 2019*.

Beauducel, F., Nurnaning, A., Iguchi, M., Fahmi, A. A., Nandaka, M. A., Sumarti, S., et al. (2014). Real-time source deformation modeling through GNSS permanent stations at Merapi volcano (Indonesia). In *AGU Fall Meeting Abstracts*.

Boudoire, G., Brugier, Y.-A., Di Muro, A., Wörner, G., Arienzo, I., Metrich, M., et al. (2019). Eruptive activity on the western flank of Piton de la Fournaise (La Réunion Island, Indian Ocean): Insights on magma transfer, storage and evolution at an oceanic volcanic island. *Journal of Petrology*, *60*(9), 1717–1752.

Boudoire, G., Di Muro, A., Liuzzo, M., Ferrazzini, V., Peltier, A., Gurrieri, S., et al. (2017). New perspectives on volcano monitoring in a tropical environment: Continuous measurements of soil CO2 flux at Piton de la Fournaise (La Réunion Island, France). *Geophysical Research Letters*, *44*, 8244–8253. https://doi.org/10.1002/2017GL074237

Boudoire, G., Liuzzo, M., Di Muro, A., Ferrazzini, V., Michon, L., Grassa, F., et al. (2017). Investigating the deepest part of a volcano plumbing system: Evidence for an active magma path below the western flank of Piton de la Fournaise (La Réunion Island). *Journal of Volcanology and Geothermal Research*, *341*, 193–207.

Brenguier, F., Shapiro, N. M., Campillo, M., Nercessian, A., & Ferrazzini, V. (2007). 3-D surface wave tomography of the Piton de la Fournaise volcano using seismic noise correlations. *Geophysical Research Letters*, *34*, L02305. https://doi.org/10.1029/2006GL028586

Cannavò, F., Camacho, A. G., González, P. J., Mattia, M., Puglisi, G., & Fernández, J. (2015). Real time tracking of magmatic intrusions by means of ground deformation modeling during volcanic crises. *Scientific Reports*, *5*, 10970.

Cayol, V., & Cornet, F. H. (1998). Three-dimensional modeling of the 1983–1984 eruption at Piton de la Fournaise Volcano, Réunion Island. *Journal of Geophysical Research*, *103*(B8), 18,025–18,037.

Desai, S., Bertiger, W., Garcia-Fernandez, M., Haines, B., Murphy, D., Selle, C., et al. (2014). Status and plans at the JPL IGS analysis center. In *Intl. GNSS Service 2014 Workshop Compendium, Ed. IGS Central Bureau*, Jet Propul. Lab., Calif. Inst. of Technol. Pasadena, Calif, pp. 53.

Di Muro, A., Métrich, N., Vergani, D., Rosi, M., Armienti, P., Fougeroux, T., et al. (2014). The shallow plumbing system of Piton de la Fournaise volcano (La Reunion Island, Indian Ocean) revealed by the major 2007 caldera-forming eruption. *Journal of Petrology*, *55*(7), 1287–1315.

Duputel, Z., Lengliné, O., & Ferrazzini, V. (2019). Constraining spatio-temporal characteristics of magma migration at Piton de la Fournaise volcano from pre-eruptive seismicity. *Geophysical Research Letters*, *46*, 119–127. https://doi.org/10.1029/2018GL080895

Dzurisin, D. (2003). A comprehensive approach to monitoring volcano deformation as a window on the eruption cycle. *Reviews of Geophysics*, *41*(1), 1001. https://doi.org/10.1029/2001RG000107

Gurioli, L., Di Muro, A., Vlastélic, I., Moune, S., Thivet, S., Valer, M., et al. (2018). Integrating field, textural, and geochemical monitoring to track eruption triggers and dynamics: A case study from Piton de la Fournaise. *Solid Earth*, *9*(2), 431.

Lengliné, O., Dputel, Z., & Ferrazzini, V. (2016). Uncovering the hidden signature of a magmatic recharge at Piton de la Fournaise volcano using small earthquakes. *Geophysical Research Letters*, *43*, 4255–4262. https://doi.org/10.1002/2016GL068383

Moretti, R., Komorowski, J.-C., Ucciani, G., Moune, S., Jessop, D., de Chabalier, J.-B., et al. (2020). The 2018 unrest phase at La Soufrière of Guadeloupe (French West Indies) andesitic volcano: Scrutiny of a failed but prodromal phreatic eruption. *Journal of Volcanology and Geothermal Research*, *393*, 106,769. https://doi.org/10.1016/j.jvolgeores.2020.106769

Nikkhoo, M., Walter, T. R., Lundgren, P. R., & Prats-Iraola, P. (2016). Compound dislocation models (CDMs) for volcano deformation analyses. *Geophysical Journal International*, *208*, 877–894.

Peltier, A., Bachèlery, P., & Staudacher, T. (2009). Magma transport and storage at Piton de La Fournaise (La Réunion) between 1972 and 2007: A review of geophysical and geochemical data. *Journal of Volcanology and Geothermal Research*, *184*(1-2), 93–108.

Peltier, A., Beauducel, F., Villeneuve, N., Ferrazzini, V., Di Muro, A., Aiuppa, A., et al. (2016). Deep fluid transfer evidenced by surface deformation during the 2014–2015 unrest at Piton de la Fournaise volcano. *Journal of Volcanology and Geothermal Research*, *321*, 140–148.

Peltier, A., Villeneuve, N., Ferrazzini, V., Testud, S., Hassen Ali, T., Boissier, P., & Catherine, P. (2018). Changes in the long-term geophysical eruptive precursors at Piton de la Fournaise: Implications for the response management. *Frontiers in Earth Science*, *6*, 104.

Prôno, E., Battaglia, J., Monteiller, V., Got, J.-L., & Ferrazzini, V. (2009). *P*-wave velocity structure of Piton de la Fournaise volcano deduced from seismic data recorded between 1996 and 1999. *Journal of Volcanology and Geothermal Research*, *184*(1-2), 49–62.

Roult, G., Peltier, A., Taisne, B., Staudacher, T., Ferrazzini, V., Di Muro, A., & OVPF (2012). A new comprehensive classification of the Piton de la Fournaise activity spanning the 1985–2010 period. Search and analysis of short-term precursors from a broad-band seismological station. *Journal of Volcanology and Geothermal Research*, *241*, 78–104.

Segall, P. (2010). *Earthquake and volcano deformation*: Princeton University Press.

Tarantola, A. (2006). Popper, Bayes and the inverse problem. *Nature Physics*, *2*(8), 492–494.

Tibaldi, A. (2015). Structure of volcano plumbing systems: A review of multi-parametric effects. *Journal of Volcanology and Geothermal Research*, *298*, 85–135.

Toutain, J.-P., Bachelery, P., Blum, P. A., Cheminée, J. L., Delorme, H., Fontaine, L., et al. (1992). Real time monitoring of vertical ground deformations during eruptions at Piton de la Fournaise. *Geophysical Research Letters*, *19*(6), 553–556.

Williams, C. A., & Wadge, G. (1998). The effects of topography on magma chamber deformation models: application to Mt. Etna and radar interferometry. *Geophysical Research Letters*, *25*(10), 1549–1552.